Power scaling of laser diode pumped Pr^{3+}:$LiYF_4$ cw lasers: efficient laser operation at 522.6 nm, 545.9 nm, 607.2 nm, and 639.5 nm

Teoman Gün,* Philip Metz, and Günter Huber

Institut für Laser-Physik, Universität Hamburg, 22761 Hamburg, Germany
**Corresponding author: tguen@physnet.uni-hamburg.de*

Received January 3, 2011; accepted January 31, 2011;
posted February 16, 2011 (Doc. ID 140151); published March 15, 2011

We report efficient cw laser operation of laser diode pumped Pr^{3+}-doped $LiYF_4$ crystals in the visible spectral region. Using two InGaN laser diodes emitting at $\lambda_P = 443.9$ nm with maximum output power of 1 W each and a 2.9-mm-long crystal with a doping concentration of 0.5%, output powers of 938 mW, 418 mW, 384 mW, and 773 mW were achieved for the laser wavelengths 639.5 nm, 607.2 nm, 545.9 nm, and 522.6 nm, respectively. The maximum absorbed pump powers were approximately 1.5 W, resulting in slope efficiencies of 63.6%, 32.0%, 52.1%, and 61.5%, as well as electro-optical efficiencies of 9.4%, 4.2%, 3.8%, and 7.7%, respectively. Within these experiments, laser diode-pumped laser action at 545.9 nm was demonstrated for what is believed to be the first time.

OCIS codes: 140.3480, 140.3580, 140.5680, 140.7300.

In recent years, considerable interest has emerged in the development of efficient laser sources emitting in the visible spectral range. The perspectives for such devices lie in the development of color displays, microsized projectors, and holographic and lithographic techniques, as well as in biomedical or quantum optical applications. One of the most promising candidates within the rare earth ions is trivalent praseodymium (Pr^{3+}), offering several transitions with high cross sections ($\approx 10^{-19}$ cm^2) in the blue (≈480 nm), green (≈520 nm), orange (≈605 nm), red (≈640 nm), and deep red (≈695 nm, ≈720 nm) spectral regions. During the past decade, efficient cw laser action has been demonstrated by exciting Pr^{3+} doped host materials by blue emitting pump sources such as InGaN laser diodes (LDs) or optically pumped semiconductor lasers (OPSL) [1–4]. Since most oxide hosts have high phonon energies, strong nonradiative decays from the upper laser levels $^3P_0$ and $^3P_1$ to the $^1D_2$ level occur, resulting in a depopulation of the upper laser level. Furthermore, in oxide hosts with relatively low bandgaps, excited state absorption from the upper laser level leads to an efficient decrease in the inversion density of the laser levels. Thus, cw operation at room temperature has been demonstrated only in the red and deep-red spectral range in perovskites and other oxides with a large bandgap [5–7].

Pr^{3+}-doped fluorides, particularly Pr^{3+}:$LiYF_4$, have been found to be the most promising materials for solid state laser emission in the visible spectral range [8]. The most efficient way for exciting Pr^{3+}:$LiYF_4$ crystals is pumping with InGaN LDs emitting at 443.9 nm [1]. Advances in their development have led to steadily increasing output powers of Pr^{3+} lasers [3]. Recently, a maximum output power of 358 mW with a maximum slope efficiency η_s of 54% has been demonstrated in the green spectral range at 522.6 nm by using LDs with 1 W output power and beam quality factors of $M_x^2 \approx 1.4$ and $M_y^2 \approx 5.8$ [9]. In this Letter, we report the highest slope efficiencies and output powers obtained for InGaN LD-pumped cw Pr^{3+}:$LiYF_4$ in the visible spectral range. In addition, the results of the first laser action based on LD-pumped Pr^{3+}:$LiYF_4$ at 545.9 nm are presented.

The spectroscopic properties of Pr^{3+}-doped $LiYF_4$ crystals regarding polarized absorption and emission are well known [10–12]. The peak absorption cross sections of the transitions from the ground state $^3H_4$ to the ^3P_J multiplet are higher in case of π-polarized light ($\mathbf{E}\|c$) with values of 8.9×10^{-20} cm^2, 6.3×10^{-20} cm^2, and 17.0×10^{-20} cm^2 for the wavelengths 443.9 nm, 468.6 nm, and 479.2 nm, respectively [8]. Exciting the Pr^{3+}:$LiYF_4$ crystal by a LD emitting at 443.9 nm leads to an emission in the visible spectral range due to the transitions from the ^3P_J multiplet to the energetically lower multiplets ^3F_J and ^3H_J. Figure 1 shows the corresponding polarization-dependent emission cross sections calculated by the Füchtbauer–Ladenburg method [13,14]. The highest emission cross sections are present in the red (639.5 nm), orange (607.2 nm), and blue (479.2 nm) spectral range, while the transitions in the green spectral range (522.6 nm, 545.9 nm) have emission cross sections that are 1 order of magnitude lower (Fig. 1).

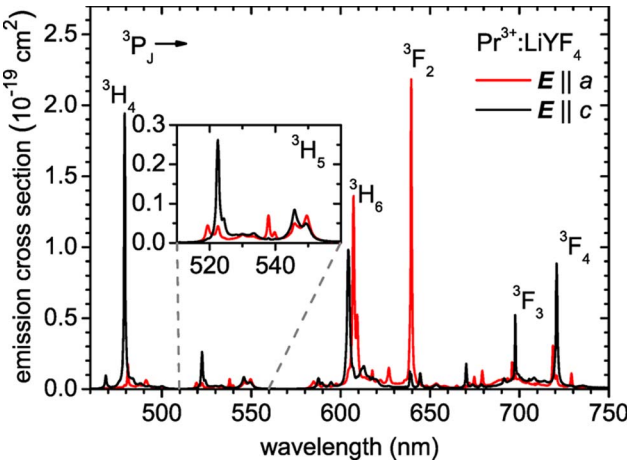

Fig. 1. (Color online) Polarization-dependent emission cross sections of a Pr^{3+}-doped $LiYF_4$ crystal using InGaN LDs as excitation source.

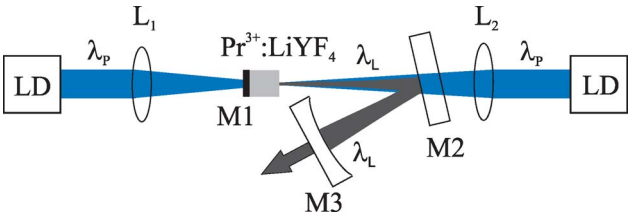

Fig. 2. (Color online) Schematic setup of the LD-pumped Pr^{3+}:$LiYF_4$ lasers.

In order to decrease the probability of possible nonradiative cross-relaxation processes, Pr^{3+}:$LiYF_4$ crystals with a low doping concentration of Pr^{3+} ions are required [15,16]. Therefore, a 2.9 mm long sample with a dopand concentration of 0.5 at.% Pr^{3+} in the crystal was used in the laser experiments, resulting in an absorption coefficient of about 6.2 cm^{-1}. Figure 2 displays the laser setup for the experiments at different laser transitions. The Pr^{3+}:$LiYF_4$ laser crystal is pumped by two LDs emitting at $\lambda_P = 443.9$ nm with a maximum output power of 1 W each. Beam collimation and shaping of the LD radiation was accomplished using a spherical lens with a focal length of 4.5 mm as well as an anamorphic cylindrical lens pair. The lenses $L_{1,2}$ of 40 mm focal length were used to focus the pump beams into the laser crystal. The singly folded cavity (V-type cavity) consisted of output couplers M3 for the laser wavelength λ_L with a radius of curvature of 50 mm, a coating M1 on the crystal as an input coupler (AR at λ_P, HR at λ_L), and a plane-folding input coupler M2. The beam waist diameter inside the crystal was approximately 80 μm. Figure 3 shows the laser performance of LD-pumped Pr^{3+}:$LiYF_4$ lasers operating at different laser transitions in the visible spectral range. At an absorbed pump power of about 1.5 W, output powers of up to 773 mW at $\lambda_L = 522.6$ nm, 384 mW at $\lambda_L = 545.9$ nm, 418 mW at $\lambda_L = 607.2$ nm, and 938 mW at $\lambda_L = 639.5$ nm were generated, resulting in slope efficiencies η_s of 61.5%, 52.1%, 32.0%, and 63.6%, respectively. The corresponding laser thresholds are listed in Fig. 3. All given data refer to the totally outcoupled power from the resonator at the mirrors M1-M3. The mirrors M1-M3 have, in sum, a net transmission T_{OC} of about 1.28%, 2%, 3.38%, and 2.46% for $\lambda_L = 522.6$ nm, 545.9 nm, 607.2 nm, and 639.5 nm, respectively, whereas the main part of the power was coupled out at mirror M3. The outcoupled power at M3 was 760 mW for $\lambda_L = 522.6$ nm, 383 mW for $\lambda_L = 545.9$ nm, 416 mW for $\lambda_L = 607.2$ nm, and 877 mW for $\lambda_L = 639.5$ nm. Table 1 summarizes all results obtained from the V-type cavity.

The internal round-trip losses L_i are primarily dependent on the scattering losses caused by the crystal and the mirrors M1-M3. For very low scattering losses in the crystal, determination of the total losses L_i by varying

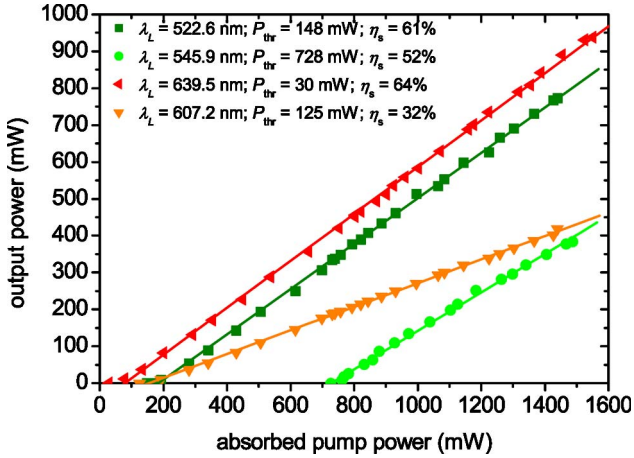

Fig. 3. (Color online) Power characteristics of InGaN LD-pumped Pr^{3+}:$LiYF_4$ lasers operating at the transitions $\lambda_L = 522.6$ nm, 545.9 nm, 607.2 nm, and 639.5 nm.

the output couplers and applying the Findlay–Clay [17] or Caird [18] methods is not reasonable and reliable. Therefore, the maximum internal losses were calculated from the measured slope efficiencies η_s and the Stokes factor $\eta_Q = \lambda_P/\lambda_L$, where the branching ratio from the pump level $^3P_2$ to the upper laser level, as well as the overlap efficiency of the pumped volume and the laser mode, have been assumed to be 1. The slope efficiencies, Stokes factors, and calculated minimum outcoupling efficiencies $\eta_{C,\min}$ are also presented in Table 1. The maximum internal round-trip losses $L_{i,\max}$ are calculated from $\eta_{c,\min}$. Resulting from scattering at the crystal as well as on the surfaces of the mirrors, the losses are increasing with decreasing laser wavelength λ_L. The high loss of the $^3P_0 \rightarrow {}^3H_5$ transition at 545.9 nm is due to the lower quality of the output coupler M3.

The low slope efficiency and the high absorbed threshold pump power P_{thr} of the laser transition $^3P_0 \rightarrow {}^3H_6$ at $\lambda_L = 607.2$ nm results from reabsorption losses due to the transition from the ground state to the $^1D_2$ level [8]. Thus, the estimated maximum losses $L_{i,\max}$ of 1.0% for this transition consist of the maximum round-trip losses and the reabsorption losses. The value of 1.0% for the maximum losses $L_{i,\max}$ was determined from the power characteristic of a laser at 607.2 nm with an output coupling of $T_{OC} = 0.76\%$ and a slope efficiency of 31.0%. The maximum round trip losses $L_{i,\max}$ without any reabsorption losses should be comparable to the losses of the red transition $^3P_0 \rightarrow {}^3F_2$. Considering Rayleigh-scattering the maximum round trip losses $L_{i,\max}$ can be estimated to be 0.3%.

The Pr^{3+}:$LiYF_4$ laser beams have been characterized spatially. They show no astigmatism or ellipticity (Fig. 4).

Table 1. Summary of Pr^{3+}:$LiYF_4$ Laser Results as a Function of the Emission Wavelength, with Stokes Factor η_Q, Minimum Outcoupling Efficiency $\eta_{C,\min}$, and Maximum Internal Round Trip Losses $L_{i,\max}$

λ_L (nm)	T_{OC} (%)	P_{thr} (mW)	$P_{\max}$ (mW)	P_{abs} (mW)	η_s (%)	η_Q (%)	$\eta_{C,\min}$ (%)	$L_{i,\max}$ (%)
522.6	1.28	148	773	1440	61.5	84.9	72.3	0.49
545.9	2.00	728	384	1488	52.1	81.3	64.1	1.12
607.2	3.38	125	418	1440	32.0	73.1	42.5	1.03
639.5	2.46	30	938	1551	63.6	69.4	91.6	0.23

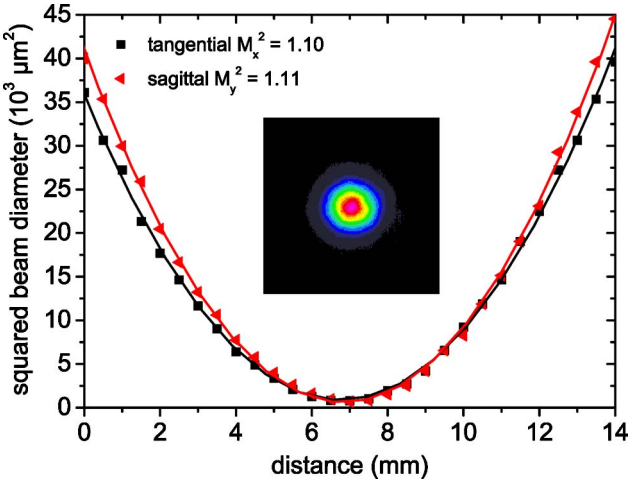

Fig. 4. (Color online) Caustic and beam profile of the Pr^{3+}:$LiYF_4$ laser operating at $\lambda_L = 522.6\,\mathrm{nm}$.

The beam quality factors of the Gaussian-shaped beams have been determined to be about $M_x^2 \approx M_y^2 \approx 1.1$. Figure 4 displays the squared beam diameter with respect to the position along the beam axis for the laser beam at $\lambda_L = 522.6\,\mathrm{nm}$.

In conclusion, we have demonstrated the most efficient LD-pumped cw laser operation at room temperature in a Pr^{3+}:$LiYF_4$ crystal on several transitions in the green, orange, and red spectral range, with the highest reported slope efficiencies and output powers for all transitions. The results are summarized in Table 1. The measured slope efficiencies are almost as high as the theoretically possible maximum slope efficiency, which is given by the Stokes factor.

Improvement of the laser performance, especially at the transition $^3P_0 \rightarrow {}^3H_5$, can be expected by optimization of the transmissivity and quality of the output coupler. However, efficient laser emission by pumping with two LDs has been obtained at the transition $^3P_0 \rightarrow {}^3H_5$ ($\lambda_L = 545.9\,\mathrm{nm}$), which has an emission cross section of $8.4 \times 10^{-21}\,\mathrm{cm}^2$. Therefore, laser operation at other wavelengths according to the emission spectrum in Fig. 1 can be realized by using a birefringent filter in order to tune the laser wavelength. Blue InGaN LDs with higher output powers, which can be expected to become available in the near future, would lead to a relatively broad tunability range in the visible spectral range.

This work was supported by the German Research Foundation (DFG) through Research Training Group 1355 and the Joachim Herz Stiftung. We wish to acknowledge COHERENT Lübeck GmbH for providing an InGaN LD.

References

1. A. Richter, E. Heumann, E. Osiac, and G. Huber, Opt. Lett. **29**, 2638 (2004).
2. A. Richter, E. Heumann, G. Huber, V. Ostroumov, and W. Seelert, Opt. Express **15**, 5172 (2007).
3. F. Cornacchia, A. D. Lieto, M. Tonelli, A. Richter, E. Heumann, and G. Huber, Opt. Express **16**, 15932 (2008).
4. H. Okamoto, K. Kasuga, I. Hara, and Y. Kubota, Opt. Express **17**, 20227 (2009).
5. T. Danger, A. Bleckmann, and G. Huber, Appl. Phys. B **58**, 413 (1994).
6. M. Fechner, A. Richter, N.-O. Hansen, A. Petrosyan, K. Petermann, and G. Huber, in *CLEO-Europe EQEC*, OSA Technical Digest Series, (Optical Society of America, 2009), paper CA6 3.
7. M. Fibrich, H. Jelinkova, J. Sulc, K. Nejezchleb, and V. Skoda, Appl. Phys. B **97**, 363 (2009).
8. A. Richter, *Laser Parameters and Performance of Pr^{3+}-doped Fluorides Operating in the Visible Spectral Region* (Cuvillier Verlag, 2008).
9. N.-O. Hansen, A. Bellancourt, U. Weichmann, and G. Huber, Appl. Opt. **49**, 3864 (2010).
10. L. Esterowitz, F. J. Bartoli, and R. E. Allen, Phys. Rev. B **19**, 6442 (1979).
11. J. L. Adam, W. A. Sibley, and D. R. Gabbe, J. Lumin. **33**, 391 (1985).
12. M. Laroche, J.-L. Doualan, J. M. S. Girard, and R. Moncorge, J. Opt. Soc. Am. B **17**, 1291 (2000).
13. H. P. Weber, P. F. Liao, and B. C. Tofield, IEEE J. Quantum Electron. **QE-10**, 563 (1974).
14. G. Huber, W. W. Krühler, W. Bludau, and H. G. Danielmeyer, J. Appl. Phys. **46**, 3580 (1975).
15. J. Hegarty, D. L. Huber, and W. M. Yen, Phys. Rev. B **25**, 5638 (1982).
16. P. J. Deren, A. Bednarkiewicz, R. Maihou, and W. Strek, Mol. Phys. **101**, 951 (2003).
17. D. Findlay and R. A. Clay, Phys. Lett. **20**, 277 (1966).
18. J. A. Caird, S. A. Payne, P. R. Staver, A. J. Ramponi, L. L. Chase, and W. F. Krupke, IEEE J. Quantum Electron. **24**, 1077 (1988).